ChemComm

FEATURE ARTICLE

View Article Online
View Journal | View Issue

Cite this: *Chem. Commun.*, 2017, 53, 4429

Triplet transport in thin films: fundamentals and applications

Xin Li and Ming Lee Tang*

Received 1st February 2017,
Accepted 23rd March 2017

DOI: 10.1039/c7cc00861a

rsc.li/chemcomm

Triplet excitons are key players in multi-excitonic processes like singlet fission and triplet–triplet annihilation based photon upconversion, which may be useful in next-generation photovoltaic devices, photocatalysis and bioimaging. Here, we present an overview of experimental and theoretical work on triplet energy transfer, with a focus on triplet transport in thin films. We start with the theory describing Dexter-mediated triplet energy transfer and the fundamental parameters controlling this process. Then we summarize current experimental methods used to measure the triplet exciton diffusion length. Finally, the use of hierarchically ordered structures to improve the triplet diffusion length is presented, before concluding with an outlook on the remaining challenges.

Triplet excitons are usually forsaken in favor of their singlet counterparts, whether in nature or in optoelectronic devices. For example, in higher plants, photosystem II non-photochemically quenches potential triplets by rearranging the light harvesting proteins to minimize the production of singlet oxygen, which is damaging to cells;[1] in organic light-emitting diodes (OLEDs), triplet excitons created by charge injection are converted to emissive singlet states by thermally activated delayed fluorescence (TADF)[2–5] or through spin–orbit coupling in organometallic compounds.[6–9] Despite being overlooked, triplet excitons play a key role in multi-excitonic processes like singlet fission and triplet–triplet annihilation (TTA), which are plausible ways of redistributing the energy contained in the solar spectrum. Through singlet fission, a photon of high energy is split into two triplet excitons of lower energy, thus allowing the energy lost in the thermalization of photons more energetic than the bandgap of a semiconductor-based solar cell to be captured.[10–13] In a related process, near infrared (NIR) radiation currently transmitted through solar cells can be harnessed through photon upconversion mediated *via* triplet fusion.[14–16] Either of these photon up- or down-conversion processes could potentially overcome the Shockley–Queisser limit and improve the power conversion efficiency (PCE) of solar cells by as much as 44% under one sun conditions.[17]

These processes are efficient in certain organic semiconductors which, like colloidal semiconductor nanocrystals, are amenable to solution-based, roll-to-roll processing for potentially inexpensive, flexible optoelectronic devices.[18,19] Quantum-confined semiconductor NCs have dark excitonic states responsive to magnetic fields in thermal equilibrium with their dipole allowed bright states at room temperature.[20] This triplet-like character stems from a non-zero exchange term resulting from the Wannier excitons in the bulk being confined at the nanoscale. Excitons

Chemistry Department, University of California, Riverside, CA 92507, USA. E-mail: mltang@ucr.edu; Tel: +951-827-5964

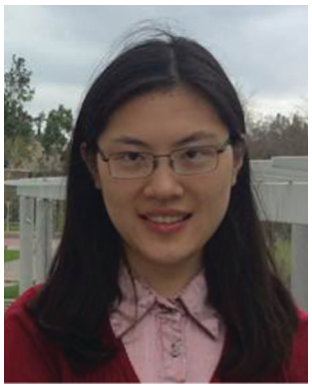

Xin Li

Xin Li received her BS degree in chemistry from Xiamen University, China in 2012. She is currently pursuing her PhD in physical chemistry under the guidance of Prof. Ming Lee Tang at University of California, Riverside. Her work focuses on designing inorganic semiconductor nanocrystals and organic molecules as hybrid materials for photon upconversion.

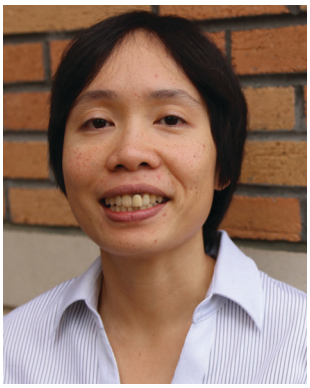

Ming Lee Tang

Ming Lee Tang is currently an assistant professor of chemistry at the University of California, Riverside. She earned her PhD in 2009 under the guidance of Prof. Zhenan Bao at Stanford University and carried out her post-doctoral research with Prof. A. Paul Alivisatos and Jeffrey R. Long at the University California, Berkeley. The Tang group works on designer ligands for functional nanocrystals.

are neutral excited states with Coulombically bound electron–hole pairs. Excitons with a net spin of zero or one are termed singlet or triplet excitons, respectively. Förster-type dipole–dipole coupling has traditionally been used to describe energy transfer between organic molecules and inorganic NCs, but recently, triplet energy transfer (TET) across this interface has been demonstrated.[21,22] Efficient TET from NCs to acene emitters has resulted in state-of-the-art photon upconversion quantum yields (QYs) under sub-solar excitation densities, even for NIR radiation.[15] In fact, the large extinction coefficient and size-dependent bandgaps of semiconductor NCs make them good sensitizers of molecular triplet states. However, an ongoing challenge in this field is to translate these encouraging results from solution into commercially relevant thin films, ideally made by low-cost printing methods.

Therefore, it would be interesting to fabricate thin films that can harness triplet excitons created by singlet fission, charge-transfer (CT) states at the polymer:fullerene interface,[23–29] or nanocrystal photosensitization,[30–36] and extract the energy contained in these excitons either through TTA *via* photon upconversion or improved PCEs in solar cells. While singlet fission enhanced organic solar cells have been demonstrated, any improvement in the PCE of the solar cell by the enhanced external quantum efficiency (EQE) from the down-converted photons was offset by the poor exciton or charge transport in existing thin films.[12] Efficient triplet exciton transport within the thin film might be one of the ways to use singlet fission to overcome the Shockley–Queisser limit. In this feature article, we consider prior work characterizing triplet diffusion in thin films, reports of thin films with large triplet diffusion lengths and potential directions for future work. We start with the mechanism of TET, summarize techniques to characterize triplet diffusion lengths in the thin film, discuss efforts to increase TET by introducing ordered structures, and end with possible implications on improving triplet diffusion.

I. Dexter transport describes triplet exciton migration

One particularly compelling reason to consider triplet excitons is the fact that there is no fundamental limit to their diffusion length. This is not the case with singlet excitons.[37] As shown in Fig. 1, excitons are tightly bound electron–hole pairs that typically occur in organic or artificial molecules like nanocrystals, where excited electronic states with a net spin of zero or one are labelled singlets or triplets, respectively. For singlet-excited states, increasing the dipole moment increases the Förster radius, thus enhancing resonance energy transfer. However, this also increases the radiative rate, decreasing the lifetime of the singlet exciton. This trade-off results in a maximal diffusion length for singlets, calculated by Yost *et al.* to be about ~100 nm for crystalline tetracene.[37] There is no such limitation for triplet excitons, because the diffusion coefficient and lifetime are not directly related. Triplet excitons in free molecules typically have inherently long microsecond lifetimes, due to spin-forbidden recombination to the ground state.

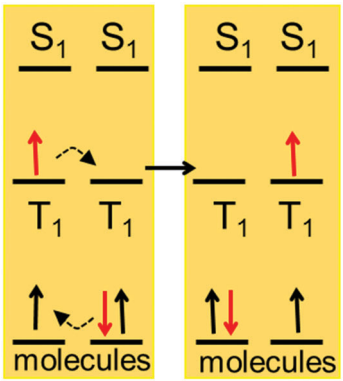

Fig. 1 Triplet energy transfer (TET) can be considered as the correlated transfer of two electrons.

The triplet diffusion coefficient is governed by the wavefunction overlap between the donor and acceptor species, or Dexter energy transfer, *i.e.* the correlated exchange of two electrons between nearest neighbors.[38] Therefore, the migration of triplet excitons can be described as a random walk. The diffusion length is defined as the root-mean-square displacement of a particle from its initial position during this diffusion process, as given below:

$$L_{\mathrm{D}} = \sqrt{\frac{\sum \mathrm{d}L_i^2}{N}} = \sqrt{2ZD\tau} \quad (1)$$

where $\mathrm{d}L_i$ is the displacement of an exciton i from its original position, N is the total number of excitons, D is the diffusion constant, τ is the lifetime of the triplet exciton and Z is equal to 1, 2 or 3 which corresponds to one-, two- or three-dimensional diffusion, respectively.[39] In fact, the factor of two is usually omitted in many scientific publications, leading to:

$$L_{\mathrm{D}} = \sqrt{ZD\tau} \quad (2)$$

The exciton diffusion constant, D, in eqn (2) can be estimated using the Smoluchowski–Einstein theory of random walks.[40] In a simple cubic lattice model where a particle is surrounded by six neighbors with an interparticle spacing a, the diffusion is assumed to be isotropic and limited to interactions with these six nearest neighbors, leading to:

$$D = \frac{a^2}{6\tau_{\mathrm{H}}} \quad (3)$$

where τ_{H} is the hopping time constant, *i.e.* the time constant for Dexter energy transfer. Combining eqn (2) and (3), the Dexter-mediated diffusion length is:

$$L_{\mathrm{D}} = \sqrt{\frac{Za^2\tau}{6\tau_{\mathrm{H}}}} \quad (4)$$

However, $1/\tau_{\mathrm{H}}$ in eqn (4), the rate of triplets hopping from site to site, or the rate of Dexter energy transfer, can be estimated using Marcus theory:[38,41–44]

$$\frac{1}{\tau_{\mathrm{H}}} = k_{\mathrm{Dexter}} = \frac{|J_{\mathrm{DA}}{}^2|}{\hbar}\sqrt{\frac{\pi}{\lambda k_{\mathrm{B}}T}}\exp\left[-\frac{\lambda}{4k_{\mathrm{B}}T}\left(1+\frac{\Delta G}{\lambda}\right)^2\right] \quad (5)$$

where $\hbar$ is Planck's constant, J_{DA} is the electronic coupling between the donor and acceptor, λ is the reorganization energy, T is the temperature, k_B is the Boltzmann constant and ΔG is the difference in Gibbs free energy between the donor and acceptor. The exponential dependence of the triplet diffusion length on the distance between the donor and acceptor means that shorter donor–acceptor distances can significantly improve hopping events between neighbours, thus increasing the diffusion length. Therefore, efforts promoting closer contact between donors and acceptors in various geometries, *e.g.* self-assembled structures, crystalline molecules and metal-containing frameworks *etc.*, will be discussed in Section III.

Since Dexter-type triplet transfer can be considered a correlated exchange of two charges (Fig. 1), the same structure–property relationships governing charge transport in organic semiconductors apply to both TET and charge transfer from triplet excitons. It has been found that the rate of triplet transfer is proportional to the product of the diffusivity of the electrons and holes in amorphous films, in organic crystals, and in solution, provided the molecular reorganization energy is taken into account.[44–47] Closs, Scholes, and others have shown that the rate of TET can be estimated from the product of the rate of electron transfer and hole transfer.[46] As shown in Fig. 2, Scholes *et al.* showed that during TET, the excited configurations of the donor A and acceptor B, represented by Φ_1(A*B) and Φ_4(AB*), respectively, are each allowed to mix with bridging ionic configurations, Φ_2(A^+B^-) and Φ_3(A^-B^+), respectively, to form new donor and acceptor wave functions.[45] In this theory, the requisite short-range orbital overlap between the donor and acceptor is described by a 'through-configuration' exciton resonance interaction term that replaces the Dexter exchange integral. These ionic, charged intermediates result in the same exponential dependence on donor and acceptor distance, described by the original 'Dexter-type' model.[48–50] In other words, TET across short bridges with high tunnelling barriers involves either sequential or simultaneous transfer of ionic intermediates.[51] Formally, the matrix element for Dexter transfer is proportional to the square of the orbital overlap between the donor and acceptor, as shown in eqn (5), but for charge transfer, it is proportional to the orbital overlap only. In other words, the damping coefficient for Dexter energy transfer should be twice as large as that for charge transfer for a physical system with the same driving force and bridge between the donor and the acceptor.

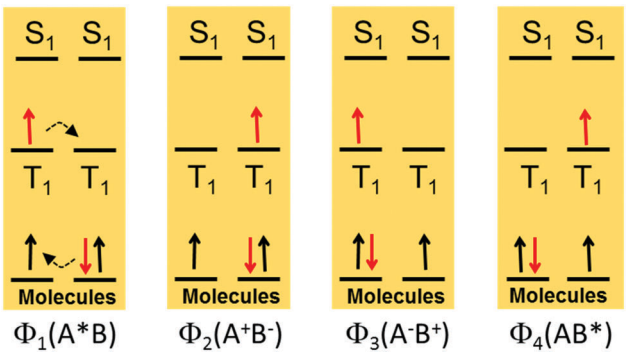

Fig. 2 Representation of four possible electronic configurations of the donor and acceptor molecules, A and B, in their excited states A* and B*, respectively. Φ_1 and Φ_4 represent locally excited configurations of molecules A (A*B) and B (AB*), respectively. Φ_2 and Φ_3 define the ionic configuration (A^+B^-) and (A^-B^+), which are to be mixed with the locally excited configurations.

II. Visualizing and quantifying triplet exciton diffusion in thin films

The reported triplet diffusion lengths in organic semiconductors span a relatively large range, from 10–20 nm up to a few micrometers.[52–56] An interfacial morphology is particularly important. For example, the long triplet diffusion lengths and lifetimes in crystalline acenes[11,57,58] can be contrasted with the fast recombination of charges derived from triplet excitons in the polymeric solar cells reported by Lacquai *et al.*[59] Thin films of tetracene have triplet diffusion lifetimes on the order of microseconds,[58,60–62] orders of magnitude larger than thin films of pentacene (15 ns).[11] Moreover, different values have been published for the same materials. For example, different triplet diffusion values in the range of 10–60 nm have been reported for 4,4′-bis(carbazol-9-yl)1,1′-biphenyl (CBP), a commonly used host material in the emissive zone of OLEDs.[63–66] Such controversy sometimes originates from the use of different measurement methods. Here we summarize the commonly used methods for measuring the triplet diffusion length and the associated problems. Unless otherwise specified, in the following section, the "sample" refers to the species whose triplet diffusion length needs to be determined, the "quenching layer" is the layer that quenches the phosphorescence signal and the heavy metal containing compounds used for reporting the presence of triplet states *via* their phosphorescence are termed the "detector" or "dopant" layer.

(1) Phosphorescence quenching

For the materials with efficient radiative decay of triplet excitons (usually organometallic compounds containing heavy metals), phosphorescence quenching methods can be directly applied.[52,67,68] For example, triplet diffusion lengths of 18.0 ± 0.6 nm and 5.7 ± 0.5 nm have been measured for amorphous films of platinum(II) octaethylporphyrin (PtOEP) (phosphorescence QY = 0.45) and platinum(II) tetraphenyltetrabenzoporphyrin (PtTPBP) (phosphorescence QY = 0.51), respectively.[52] In this method, the strongly phosphorescent material is cast as a film and then a thin quenching layer (usually composed of fullerene or TiO_2) is brought into contact with it (Fig. 3a). If the thickness of the sample layer is on the order of its triplet exciton diffusion length, then the majority of triplet excitons generated within the sample layer will diffuse to the quenching layer and phosphorescence will be quenched. Consequently, the degree of quenching can be measured from thickness-dependent time-resolved photoluminescence (PL) or steady-state PL and compared to the isolated sample film. The steady-state or time-resolved quenching data as a function of the thickness of the sample film can then be fit using appropriate models (Monte Carlo simulations

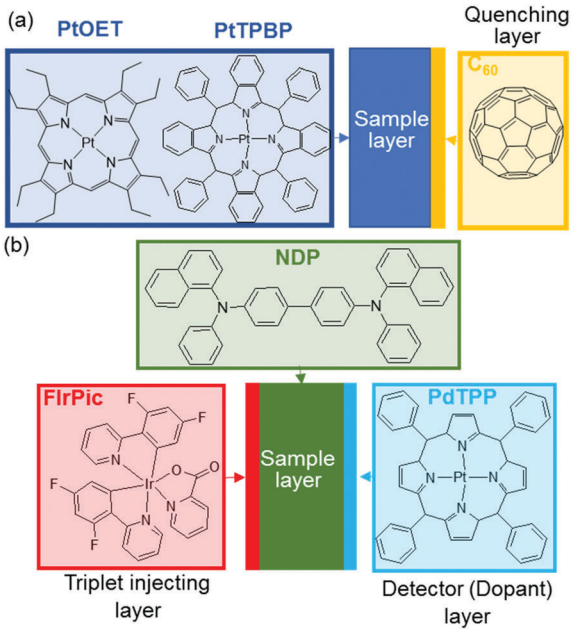

Fig. 3 Illustrations of the experimental geometry used to determine triplet diffusion lengths using (a) phosphorescence quenching and (b) remote phosphorescence sensing.

or the Stern–Volmer equation) to extract the diffusion length. We must note that triplet excitons can also be transported *via* Förster energy transfer in some heavy metal-coordinated compounds, which may complicate the analysis.[69]

(2) Remote phosphorescence sensing

When the phosphorescence QY of the sample is low, a remote phosphorescence sensing technique can come into play. By introducing a sensing layer that is heavily doped with a phosphorescent molecule, the triplet exciton can be detected (Fig. 3(b)).[63,70] To be more specific, the triplet exciton created in the sample layer diffuses into the doped layer, where energy transfer to the dopants is detected as phosphorescence. We should also note that, as the excitons diffuse, they undergo TTA which results in delayed fluorescence. Consequently, the fitting model has to involve four fitting parameters, including the exciton diffusion length, the rate of triplet–triplet annihilation, the rate of energy transfer from the sample to the phosphorescent dopant and the initial triplet density. The large number of fitting parameters and the complex theoretical model limit the accuracy and the ease of using this model.

A more straightforward method was developed by introducing a triplet injection layer on top of the sample layer and the dopant detector layer.[71] In this method, the injection and detector layer should be carefully selected such that the energy of the triplet exciton in the sample layer is in between these two layers. Thus, optically excited triplet excitons can be transferred from the injection layer to the sample layer of known thickness, then diffuse to the detection layer and be quantified by phosphorescence of the dopant. With the triplet injection layer, the initial triplet density is proportional to the intensity of the incident light and TTA can be accurately accounted for. This method ameliorates the systemic error that can be significant when TTA is not properly accounted for during the measurement. This may be the reason for the large spread of L_D values reported on the same materials in the literature, in which TTA is usually neglected.

(3) Photocurrent in solar cells

The triplet exciton diffusion length can also be measured using photocurrent modeling.[52,65,68,72–77] Here, it is important to distinguish between the contributions of triplet and singlet excitons to photocurrent. The effect of triplet–triplet annihilation also leads to inaccuracies as discussed above.

(4) Measurements in organic light-emitting diodes (OLEDs)

In OLEDs, triplet excitons are created in a charge recombination region spatially confined between the electron and hole transporting layers.[53,54,64,70,78,79] A phosphorescent dopant is added into one of the charge transporting layers at a certain distance L away from the charge recombination layer as a detector layer to optically report on the presence of triplet excitons. The dopant is selected such that TET from the sample is favorable in order for phosphorescence to be measured at the detector layer. During the measurement, the relationship between the phosphorescence intensity of dopant molecules *versus* distance L is recorded to extract the triplet exciton density. The distance-dependent profile of the triplet exciton density can be modeled to obtain the exciton diffusion length.

(5) Direct visualization of TET

Recently, a few groups have directly monitored the spatial and temporal profiles of triplet diffusion in thin films.[80–83] As shown in Fig. 4, the spatial spread of the signal at each delay time can be fitted with a Gaussian function parameterized by variance σ. The exciton diffusion length L at delay time t is then related to the exciton density characterized by variance σ,

$$L = \sigma(t) - \sigma(0) = 2Dt \quad (6)$$

enabling the diffusion constant, D, to be extracted. For the direct visualization of triplet diffusion, both time-resolved PL and transient absorption spectroscopy have been integrated with diffraction-limited resolution, as discussed in detail below:

a. Delayed luminescence. If time-resolved luminescence is monitored, the spatial spread of delayed fluorescence is measured as a function of time. Upon optical excitation, the triplet excitons generated by singlet fission or intersystem crossing can randomly hop to their nearest neighbors by Dexter energy transfer. When two diffusing triplets encounter each other, triplet fusion occurs to produce a singlet exciton, which then undergoes radiative relaxation, known as delayed fluorescence. This fluorescence can be optically detected and used as a direct probe of the triplet exciton density. Using this method, Akselrod *et al.* measured the triplet diffusion length in tetracene crystals to be about 0.61 μm with a diffusion constant of $1.35 \pm 0.01 \times 10^{-3}$ cm^2 s^{-1}.[80] They also demonstrated that the mechanism of exciton transport depends strongly on the nanoscale morphology. Note that these measurements were performed at long timescales, up to 7 μs with a temporal resolution of 100 ns. For the spatially resolved

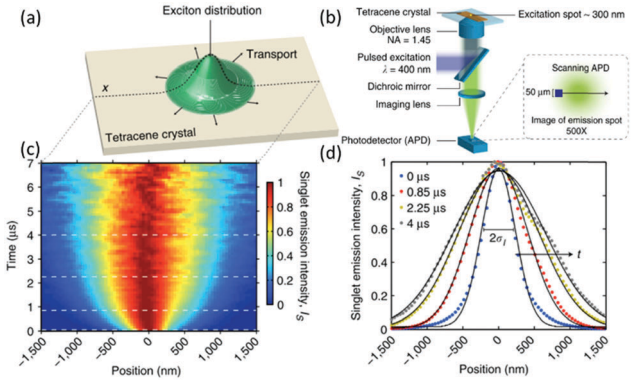

Fig. 4 Imaging tetracene exciton transport in time and space. (a) Schematic of the experimental setup showing the initial exciton distribution spreading in the plane of the crystal. (b) Schematic of the optical apparatus. The time-resolved photodetector (an avalanche photodiode) is scanned across the sample to obtain a map of emission intensity as a function of position and time. (c) Map of the emission intensity as it evolves in space and time. The distribution at a particular time has been normalized to emphasize changes in the distribution width. (d) Cross-sections of the emission intensity map at four time points showing spatial broadening of the intensity distribution. σ is the standard deviation of the Gaussian distribution. Adopted with permission from ref. 81. Copyright 2014 Nature Publishing Group.

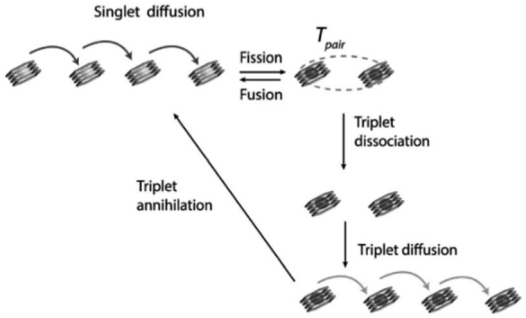

Fig. 5 The kinetics controlling singlet and triplet populations revealed by ultra-fast transient absorption measurements on tetracene films. The unprecedented spatial and temporal resolution revealed a new mechanism of singlet-mediated triplet energy transfer. Adopted with permission from ref. 83. Copyright 2016 Wiley-VCH.

dynamics of triplet diffusion at early timescales, *i.e.* picoseconds and nanosceconds, ultra-fast transient absorption measurements were elegantly employed, as discussed below.

b. Ultra-fast transient absorption measurements. Transient absorption can be used to study the dynamics of excited states in organic semiconductors. Since the absorption spectrum of the triplet exciton usually differs from that of the singlet exciton, monitoring the time evolution of their spectrally resolved optical profiles will enable the extraction of triplet diffusion parameters. Using this approach, Wan *et al.* studied the triplet diffusion dynamics in teteracene crystals at the picosecond and nanosecond timescales.[81] They selected 633 and 810 nm as the probe wavelengths to selectively monitor the singlet and triplet excitons, respectively. They estimated the diffusion constant for triplets in tetracene crystals with a time resolution of 200 fs, providing significantly more detail than the previous PL-based measurements. Data obtained at these early timescales provided evidence for a new singlet-mediated transport mechanism for triplets. In a tetracene thin film, both triplets and singlets are involved in exciton diffusion, with rapid interconversion between both species. As a result, the triplets travel much faster than expected considering that they are typically limited by Dexter transport, because they can take advantage of the dipole–dipole coupling between singlets. This new mechanism (shown in Fig. 5) increases the effective triplet exciton diffusion length to about 5.6 μm on short picosecond and nanosecond timescales.

III. Hierarchical order in harvesting triplet excitons

Ordered structures enabling efficient energy transfer along a certain direction are important for all kinds of optoelectronic devices, *e.g.* solar cells, LEDs, photodetectors, photocatalysts, *etc.* For example, it would be desirable to couple the light from a photon upconverting thin film efficiently to a solar cell or a photocatalyst. Based on eqn (5), it is essential to increase the orbital overlap between neighboring molecules in order to efficiently harvest the energy contained in triplet excitons. Therefore, here we summarize recent work implementing ordered structures for the purpose of enhancing TET. Various self-assembly methods involving small molecule design, block copolymers and long -range order enabled by frameworks like MOFs are discussed. These reports may give inspiration and shed light on future prototypes that can efficiently harvest the energy in triplet excitons.

(1) Polymer scaffolds

a. Conjugated polymers. Since Dexter transfer is the correlated exchange of two charges and can be parameterized by ionic intermediates, the extensive research regarding charge transfer in the field of conjugated polymers applies to the design of thin films with optimized morphologies for TET. Early reports established that crystalline organic semiconductors displayed better charge transport than their amorphous analogues. As a result, many conjugated polymers designed to have good charge transport properties by increasing regioregularity, π stacking or crystallinity have been reported.[84–87] However, it is also well known that polymer processing conditions greatly affect the interactions between the conjugated core. More significantly, highly disordered or even seemingly amorphous polymers have field-effect mobilities as high as their crystalline counterparts.[84,88,89]

Noriega *et al.* proposed a general model describing charge carrier transport in conjugated polymer films. They brought together relevant data (such as mobility, degree of polymerization, *etc.*) from years of research on conjugated polymers in the literature and reexamined the relationship between charge mobility and the morphology.[90] They proposed that in heterogeneous microstructures where both crystalline and amorphous areas coexist, the ordered regions are largely responsible for charge transport because there is an energy barrier for charges to move from ordered to amorphous regions across grain

boundaries. In the meantime, the chain segments connecting ordered regions provide an efficient charge transport pathway between grains, allowing charges to shuttle between each isolated crystalline aggregate. Therefore, the effect of crystallinity on charge transport in semicrystalline polymers is subject to an intrinsic and general trade-off: low molecular weight short-chain polymers improve the local crystallinity, but also suffer from poor electrical connectivity between ordered regions, thus reducing the overall mobility. Increasing the polymer crystallinity can only improve the charge transport to a limited extent due to this intrinsic trade-off. On the other hand, careful design of polymers to reduce the π–π stacking distance or increase orbital overlap can greatly improve the charge transport efficiency by enhancing transport in the local ordered regions.

b. Block copolymer templates. Many attempts have been made to use polymers to control the nano- or mesoscale separation in organic bulk heterojunctions since Friend and Heeger independently demonstrated that solvent-assisted annealing improved exciton dissociation and charge transport in PV devices.[91,92] For example, conjugated donors and acceptors covalently attached to the polymer backbone, whether alternating in a block-copolymer form or with one component pendent to a basic repeating unit, were synthesized. The motivation behind this is that the self-assembly of flexible block copolymers can be described in terms of the volume fraction, the number of statistical segment lengths and the Flory–Huggins interaction parameter of each block.[93–96] However, the rigidity of conjugated block copolymers makes it difficult to predict their morphology, especially at the donor–acceptor interface. Consequently, the performance of photovoltaic devices based on block copolymers or 'cable polymers' that have electronically active pendent groups is still low. For the latter, the low concentration of the fullerene results in a lack of control over the ratios of the donor and acceptor. More significantly, there are charge transport problems from recombination or trapping in these polymeric thin films. Perhaps this is analogous to the short-lived triplet pairs produced from intramolecular singlet fission in dimers of tetracene and pentacene. Instead of the tens of microsecond lifetimes commonly observed in isolated molecules, these dimers have triplet lifetimes on the order of nanoseconds because of enhanced recombination.[97–99] On the other hand, monolithic blocks of conjugated polymers exclusively comprising either donors or acceptors can have the degree of crystallinity, solubility, polydispersity *etc.* pre-designed by controlling the side chains and rigidity of the monomers. The best performing conjugated block copolymer consisting of P3HT donor and benzothiadiazole acceptor blocks has a PCE of 3%,[100] a factor of 4 lower than state-of-the-art OPV materials. For further insight into this sub-field, please see a recent review by Lee and Gomez.[101]

c. Rigid polymer hosts. As discussed earlier, a long triplet diffusion length can arise either from an extended exciton lifetime or from a larger diffusion coefficient, D. Monguzzi and co-workers increased the triplet exciton lifetime by embedding the molecular upconversion materials in a rigid polystyrene (PS) matrix that inhibits intramolecular relaxation.[102] This rigid PS host simultaneously minimizes the decay of the triplets by first-order processes while introducing a barrier to oxygen. The efficiency of TET was 70% of that in the diffusion-limited case in solution. Although the upconversion QY was 10× lower than the reference solution at 2.5%, the threshold intensity was reported to be around 6 mW cm^{-2}, which is close to the solar flux for the green wavelengths used for excitation.

(2) Molecular assemblies

TTA-based photon upconversion is a process where two or more lower energy photons are converted to one high-energy photon. Among reported upconversion methods, it is the only one that has demonstrated potential for harvesting incoherent photons from the sun without concentrators. Monguzzi *et al.* proposed a figure of merit for TTA-based upconversion:[103] the threshold excitation intensity, I_{th}, at which the efficiency of TTA is 0.5. They showed that:

$$I_{th} = (\alpha \Phi_{ET} 8\pi D a_0)^{-1} (\tau_T)^{-2} \quad (7)$$

where α is the donor absorption coefficient at the excitation wavelength, Φ_{ET} is the quantum efficiency of TET, D is the diffusion constant of the annihilator/emitter's triplet excited state, a_0 is the minimum distance required for the annihilation of two triplets on the acceptors (a_0 = 9 Å for DPA), and τ_T is the lifetime of triplets. Below I_{th}, the dynamics of acceptor triplet states is dominated by spontaneous nonradiative decay where TTA is inefficient. Only when the incident power is higher than I_{th}, the TTA process dominates and the upconversion QY can be maximized. Note that sunlight is ~100 mW cm^{-2} across the entire solar spectrum, and thus only a few mW cm^{-2} at the excitation wavelengths selected during experiments. Therefore, to use sunlight for photon upconversion, the TTA-based upconversion system should be carefully designed such that the I_{th} is well below solar irradiance. Based on eqn (7), it is essential to improve TET to lower I_{th}. Inspired by biological photosynthetic systems, the self-assembly of functional molecules into ordered molecular assemblies for efficient energy migration has been reported. Here we summarize some self-assembled systems that aim to improve triplet diffusion for the application of TTA-based photon upconversion.

a. Self-assembly of small molecules. So far, the most efficient molecular photon upconversion systems have been demonstrated in volatile organic solvents that conveniently eliminate triplet diffusion as the bottleneck for TET. However, practical applications require these liquid phases to be replaced, ideally with oxygen barriers. Recently, Duan *et al.* developed a nonvolatile solution that can perform photon upconversion in air.[104] Duan *et al.* functionalized the commonly used 9,10-diphenylanthracene (DPA) emitter and the Pt(II) porphyrin sensitizer with a long branched alkyl chain, molecules **1** and **2** in Fig. 6. The functionalized DPA emitter **1** containing 0.01 mol% Pt(II) sensitizer **2** exhibited blue emission upon excitation with a 532 nm green laser even in air. This system demonstrated an efficient upconversion QY of about 28%, comparable to the record 35% that was obtained from the unfunctionalized sensitizer and emitter pair in an organic solvent. The upconverted emission is still observed below the glass transition temperature, indicating

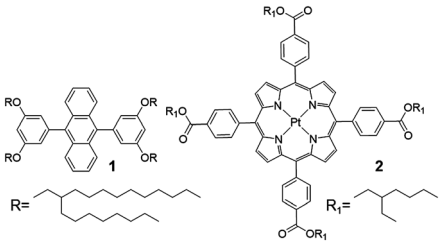

Fig. 6 Chemical structures of 9,10-diphenylanthracene (DPA) functionalized with branched alkyl chains **1** emitter and a Pt(II) porphyrin sensitizer **2** used in nonvolatile solution-based photon upconversion mediated by triplet fusion.

that triplet energy migration occurred in the glassy phase, along the electronically active π-conjugated core within the self-assembled molecules. However, the triplet diffusion constant D_T was low, on the order of 10^{-7} cm^2 s^{-1}, and the intensity threshold was relatively high at 50 mW cm^{-2}. This was ascribed to the large interchromophore distance, about 2.1 nm, between the DPA emitters, imposed by the alkyl chain. This large separation impedes the efficient migration of triplet states among DPA emitters, thus lowering the diffusion constant of triplet states.

b. Ionic liquids. In order to realize a much closer stacking of the emitter, Hisamitsu *et al.* used ionic liquids (ILs) that contain closely packed charged chromphores.[105] In their work, the sulfonated DPA anion **IL1** (Fig. 7) was used with an alkylated phosphonium countercation, eliminating alkyl chains. The excitation of the Pt(II) porphyrin sensitizer **PtOEP** that was dissolved in the DPA ionic liquid resulted in upconverted violet emission detected at around 450 nm. Here the inter-molecular distance between DPA emitters is much closer than those in the self-assembly system mentioned in Section III(2)a above. The excitation intensity threshold was successfully reduced to a low

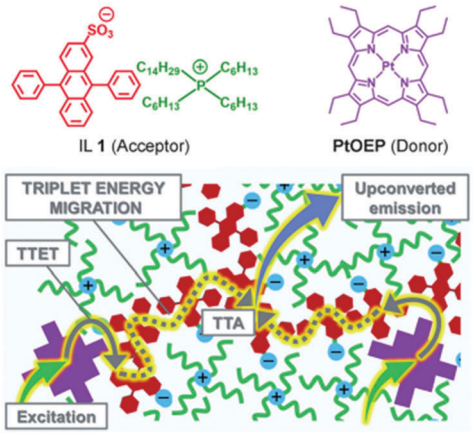

Fig. 7 Schematic representation of triplet energy migration in ionic liquids. The purple block is the sensitizer, Pt(II) octaethylporphyrin (**PtOEP**). Upon excitation, the triplet exciton generated in the sensitizer can transfer to 9,10-diphenyl anthracene (**DPA**) derivatives **IL1** (shown as red blocks, and green wavy lines indicate their counter ions) through triplet-TET (TTET). Instead of diffusion, the triplet excitons migrate along the ionic liquid matrix defined by **IL1**. Once two triplet excitons encounter each other, upconverted light is emitted through triplet–triplet annihilation (TTA). Adopted with permission from ref. 106. Copyright 2015 Wiley-VCH.

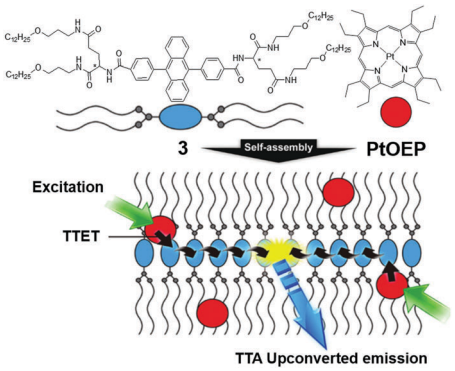

Fig. 8 Schematic illustration of the self-assembled membrane structure. An emitter molecule **3** and a sensitizer molecule **PtOEP** spontaneously self-assemble in solution. Upon photoexcitation of donor molecules (**PtOEP**) by green light, donor-to-acceptor triplet–triplet energy transfer (TTET) is followed by triplet energy migration among the acceptor networks. It leads to efficient triplet–triplet annihilation between acceptor triplets and subsequent emission of the upconverted violet light. Adopted with permission from ref. 107. Copyright 2015 Nature Publishing Group.

value of 3.0 mW cm^{-2}, which was ascribed to the long triplet diffusion length (0.63 μm) and the relatively high diffusion constant of 1.16×10^{-6} cm^2 s^{-1}. Low temperature measurements showed that excitons diffuse predominantly by energy migration along the molecular assemblies rather than by molecular diffusion (Fig. 8).

c. Membranes. The self-assembly of chromophores for photon upconversion was promoted by amide group-enriched glutamate with the formation of hydrogen bond networks. Ogawa *et al.* used an amphiphilic DPA emitter, compound **3**, functionalized with a lipophilic alkyl chain linked by lipophobic L-glutamate connectors.[106] In this system, they observed a remarkable triplet diffusion constant of $D_T = 1.4 \times 10^{-5}$ cm^2 s^{-1}, which is comparable to the molecular diffusion constant of DPA in a low-viscosity solvent (1.2×10^{-5} cm^2 s^{-1}) or in an ordered anthracene crystal. With this structure, the intensity threshold was reduced to as low as 8.9 mW cm^{-2} and the upconversion QY was about 30%. One problem associated with this measurement is the use of an oxygen-sensitive sample (PtOEP and DPA in degassed THF) as a standard when reporting the photon upconversion quantum yield. Air-stable compounds with widely accepted fluorescence quantum yield values should be employed as standards instead.[107] In addition, even though the self-assembled structure was characterized on a thin film, there was no direct characterization of this self-assembly structure in solution.

They also claimed that this molecular assembly demonstrated excellent oxygen resistance: about 83% of the upconversion signal was maintained even in the presence of dissolved oxygen. The authors attributed this oxygen barrier to the presence of hydrogen bonding networks. However, another possible reason for the oxygen resistance is that oxygen may be depleted in the vicinity of the acceptors by reaction of the photo-excited molecules with singlet oxygen. Ogawa *et al.* report that the upconverted emission for their self-assembled structures exhibited a gradual increase in the first 100 seconds. This suggests that the surrounding oxygen molecules have been consumed as reported elsewhere.[108,109]

Self-assembly employing amphiphilic acceptors that can be used in aqueous media was also reported.[110] This time, hydrophilic quaternary ammonium groups were functionalized at both ends of the DPA emitter through an amine bond. Hydrogen bond networks were observed in the hydrophobic interior. This compensates for the lower stacking ability intrinsic to the structure of DPA. The upconversion QY and diffusion constant (D) were measured to be $\sim$6.5% and $\sim 1.4 \times 10^{-4}$ cm^2 s^{-1}, respectively.

We note that in these examples of self-assembled molecular systems, the diffusion coefficients are estimated using eqn (7), where the Φ_{ET} is assumed to be one and τ_T, the lifetime of the triplet states, is obtained by monitoring the photoluminescence decay of the upconverted emission. When measuring τ_T, the relation $I_{UC}(t) \propto \exp(-t/\tau_{UC}) = \exp(-2t/\tau_T)$ was used, where τ_{UC} and τ_T are the lifetimes of the emission from the acceptor's singlet and triplet state, respectively. Since the diffusion coefficient is inversely related to the square of τ_T, accurate measurements of τ_T are highly desirable for a reliable determination of the diffusion coefficient as well as the triplet diffusion length in the molecular assembly systems.

(3) Crystalline frameworks

Metal organic frameworks (MOFs) or covalent organic frameworks (COFs) are crystalline, porous, covalently linked extended structures that may promote efficient energy transfer. The long-range order in these frameworks could potentially eliminate local variations such as traps and defects, leading to higher rates of energy transfer if the orbital overlap between the donor and acceptor is enhanced.

a. Metal organic frameworks (MOFs). The group of Wenbin Lin explored the possibility of long-range TET in MOFs by designing Ru(II) and Os(II) MOFs with bipyridyl ligands. By increasing the concentration of Os(II) complexes doped into Ru(II) MOFs, the triplet excited states of Ru(II) were readily quenched by energy migration to the Os trap sites. The energy migration was evidenced by the growth of Os(II) complex emission along with the decrease of the lifetime of Ru(II) complexes shown from time-resolved PL spectroscopy. Analysis showed that the Ru triplet state can travel about 15–55 nm over its lifetime before it is trapped on the Os(II) complexes center.[111] Using the same Ru(II) and Os(II) complex based MOFs, Kent *et al.* also showed that these MOF crystals can also be quenched oxidatively or reductively at the MOF–solution interface.[112] This system demonstrates long-range TET over several hundred nanometers. In addition, quenching by methylene blue at the MOF–solution interface is amplified by 7000-fold relative to a model complex in solution.[113] These results reveal that in these MOF systems, 'outer-sphere' electron transfer is favorable. As shown in Fig. 9, the hierarchical order within a MOF establishes certain pathways for exciton migration. Theoretical investigations showed that this incoherent hopping of triplet excitons occurs by Dexter energy transfer. In contrast to FRET, the Dexter energy transfer rates drop exponentially with distance and are strongly sensitive to the electronic coupling between the neighboring chromophores.[114]

Does Förster or Dexter energy transfer dominate in these MOFs? Depending on the composition of the building blocks,

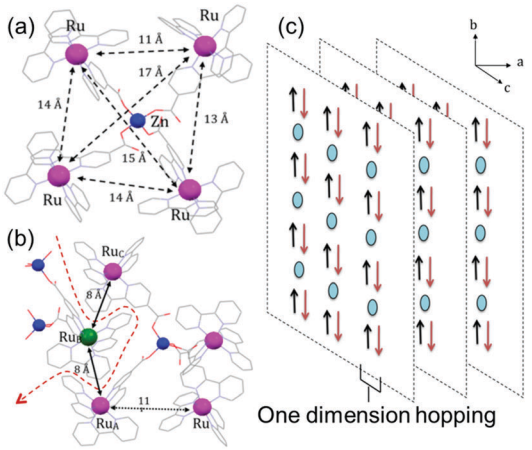

Fig. 9 Structure of the Ru-based MOF (a) within a bilayer and (b) at the bilayer–bilayer interface (dotted red line). In this MOF structure, the carboxylic acid group functionalized bispyridine ligand for Ru is linked through a tetrahedral Zn node. Therefore, each Ru center is covalently linked through a Zn-carboxylate bridge to 12 other Ru centers within the bilayer. The minimum distance between Ru atoms within the Zn–Ru_4 subunit is 11 Å. At the bilayer–bilayer interface (dotted red line), the minimum Ru–Ru distances are 8 Å (solid black lines), and there are no covalent links between the Ru centers belonging to different bilayers. Therefore, the shortest separation between Ru–Ru centers leading to the strongest electronic coupling is at the bilayer–bilayer interface, denoted as the b axis here. (c) TET in this MOF is shown to be one-dimensional along the b axis in the lattice where the electronic coupling between two Ru centers is the strongest. Each blue dot corresponds to a metal–polypyridyl centered triplet excited state. Adopted with permission from ref. 109. Copyright 2013 American Chemical Society.

both the Dexter and Förster processes occur. Experimentally, TET was observed when the Morris group impregnated Zr-based MOFs with ruthenium or osmium polypyridyl complexes, and then characterized the loading and the changes in lifetimes when compared to the original isolated organometallic compound. Theoretically, Beratan *et al.* predicted negligible Förster energy transfer due to the relatively weak transition dipole strength of the lower metal to ligand charge transfer (MLCT) singlet states.[114] In their calculations, they assumed that the lowest $Ru(bpy)_3^{2+}$ excited state consists of 10% singlet character and 90% triplet character. Furthermore, they pointed out that the vibronically broadened energy levels of the triplet states preclude coherent coupling because resonance conditions are usually satisfied when the relevant energy levels are within 0.1 meV of each other. Separately, Lin and Wang observed efficient energy transfer and exciton migration from truxene ligands in the Zn-framework to infiltrated coumarin dye molecules.[115,116] They saw a long distance through space energy migration accounting for up to 33% of energy transfer in 3D truxene-tribenzoate based Zn MOFs that have no Ru, Ir or Re ions for spin–orbit coupling. The remaining 67% was attributed to nearest-neighbor hopping of singlet excitons. In these reports, the acceptors are irregularly dispersed throughout the framework such that it is difficult to draw definite conclusions because the distribution is unknown. In addition, the MOF-based environment might perturb the nature of the excited states.

In the past year, there have been two reported attempts to harness order in a MOF framework for photon upconversion. Oldenburg *et al.* made a trilayer structure where the sensitizer (Pd(II) 5,15-diphenyl-10,20-di(4-carboxyphenyl) porphyrin light absorber) was sandwiched by the DPA light emitter held together by Zn nodes.[117] While they demonstrated relatively low threshold intensities for the linear regime in their upconversion measurements, the overall upconversion QYs were less than 0.1%, probably because the fluorescence QY of the annihilator layer was only 1.8% (*vs.* 95% for the free DPA, indicating losses *via* non-radiative decay pathways), and TET from the donor to the acceptor was severely constrained, possibly due to the lattice mismatch between the 2 layers and roughness/defects in the MOF lattice. In the meantime, Mahato *et al.* synthesized another DPA-containing MOF for photon upconversion, to take advantage of triplet exciton migration between DPA molecules that are closely assembled and aligned.[118] While the enhanced orbital overlap significantly improves the efficiency of triplet migration, it decreased the fluorescence QY of DPA, like in the work of Oldenburg and co-workers. Mahato's solution to this problem was the introduction of an energy sink for the triplet excitons, a light-harvesting layer composed of a highly fluorescent material, Coumarin 343, on the surface of MOF (Fig. 10). With this directed energy transfer to the emitter on the surface of the MOF, their photon upconversion QY was boosted from 0.35% to 2.3% and the I_{th} was 6.5 mW cm^{-2} at 532 nm, close to the solar flux at 532 nm of 1.6 mW cm^{-2}. In terms of increasing the photon upconversion QYs by maximizing the probability that triplet fusion will result in a singlet excited state, Monguzzi and Menairdi have employed perylene as the annihilator/emitter. Perylene's second excited triplet state, $E(T_2) \sim 4.0$ eV, is much larger than double the value of the first excited triplet state, $E(T_1) \sim 1.5$ eV. Hence, the probability of forming a singlet-excited state with the fusion of two triplets is one with this acceptor.

b. Covalent organic frameworks (COFs). COFs have also been used to harvest light, whether in the form of singlet or triplet, excitons. When phthalocyanines are photoexcited they decay to their triplet states within picoseconds, so COFs incorporating these building blocks demonstrate TET.[119,120] The concept of using COFs to introduce an electronic heterojunction, *e.g.* between a donor and an acceptor, has been implemented in two ways. Firstly, the donor can anchor the framework, while the acceptor (usually a C_{60} derivative) can be used to infiltrate the pores. Chen and Jiang have used click chemistry to covalently bind C_{60} to the COF after infiltration. They showed that the photoinduced triplets on the ZnPc-COF are split into radical cations in the ZnPc columns, while the radical anions end up in the C_{60} molecules within the pores.[120] Alternatively, both the donor and the acceptor can be used to build the framework, for example in the case of the phthalocyanine donor and arene diimide acceptors linked by boronate ester. Jiang and Irle argue that the photoinduced excited states on these COFs have a lifetime on the order of microseconds as indicated by the ground-state bleaching in TA spectroscopy. Further resolution of the photodynamics was inhibited by the poor solubility of the COFs.[121] In other donor–acceptor COFs, *e.g.* triphenylene-napthalene diimide,[122] shortened lifetimes given by time-resolved fluorescence spectroscopy of the donor, coupled with electron paramagnetic resonance spectroscopy, indicate enhanced photoinduced charge separation. Time-resolved microwave conductivity showed that the electron-withdrawing benzothiadiazole units within the framework could induce electron transport in a Ni-phthalocyanine COF (mobility $\sim$0.6 cm^2 V^{-1} s^{-1}).[123] TA of benzodithiophene–triphenylene COFs infiltrated with PCBM shows polaron formation supporting charge-dissociation at the interface.[124] Despite all this spectroscopic evidence of photo-induced charges created on the donor and acceptor components, it remains a challenge to extract the charges derived from these photoexcited states. In terms of photovoltaic devices, PCEs less than 1% have been reported, *e.g.* a thieno[2,3-*b*]thiophene (TT)-based COF combined with PCBM has a PCE of 0.053%,[125] while a pyrene-based COF with C_{60} has a PCE of 0.9%. The authors argue that the grain boundaries present between misaligned COF crystals in the active area inhibit charge transport, thus resulting in low PCEs.[126]

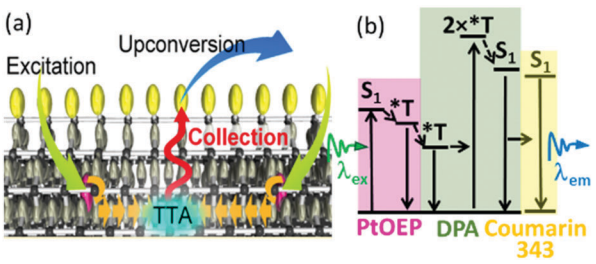

Fig. 10 (a) An anthracene-based MOF for photon upconversion that has its outer surface decorated with a highly fluorescent material as an energy sink. Triplet excitons can diffuse through the anthracene network within the MOF structure towards this outer layer that emits light. This spatially defined energy cascade enhances the upconversion quantum yield. (b) Energy diagram of the DPA-based MOF photon upconverting system involving a highly fluorescent dye (Coumarin 343) as the energy collector. Adopted with permission from ref. 115. Copyright 2016 American Chemical Society.

(4) Triplet excitons in solar cells

If the photocurrent in a solar cell is derived from triplets (*e.g. via* singlet fission), there will be a magnetic field dependence. A decrease in photocurrent at high magnetic field points to charges originating from triplet excitons, while the converse, an increase in photocurrent with large magnetic fields, implies that triplet excitons are unable to dissociate into holes and electrons, perhaps due to triplet–polaron or triplet–charge annihilation.[127,128] The 109% EQE at 670 nm in pentacene solar cells indicates that triplets from acenes can be harvested in a photovoltaic device.[12] Triplet excitons arising from singlet fission have been collected as charge in hybrid solar cells made of acenes and nanocrystals.[13,129,130] Photovoltaic cells composed of bilayers of pentacene/PbSe and TIPSEpentacene/PbX have reported PCEs of $\sim$4.8%.[13,131]

Excitonic solar cells rely on efficient light absorption, exciton formation, charge transfer state creation, charge separation, charge diffusion and collection. The microscopic mechanism by which charge separation proceeds from the transient charge transfer states is still unknown. Zhu has shown that at the

pentacene/C_{60} interface, singlet fission into triplets occurs faster than charge dissociation.[132] In 2013, Friend *et al.* reported that if the energy level of the T_1 state is lower than the CT state with triplet character, ^{3}CT, formed upon exciton dissociation, then triplet excitons become non-radiative recombination centers.[133] They showed that this can be avoided when enhanced wavefunction delocalization in the electron acceptor lowers the energy level of both the singlet and triplet charge transfer states, ^{1}CT and ^{3}CT, such that the resultant energy cascade funnels the electrons into the acceptor.

Crystallinity within the active layer significantly affects the energy level of charge transfer states. Lin *et al.* reported that the charge transfer state of a rubrene/C_{60} solar cell could be shifted by over 300 meV by simply crystallizing the as-deposited amorphous film. This made the dissociation of the triplet exciton more favorable compared to the amorphous film, thus increasing the photocurrent. A more crystalline film also has better charge transport properties due to the increased coupling between molecules.

IV. Conclusions

Triplet excitons, with their long lifetimes, can potentially be harnessed to make next-generation photovoltaic cells that exceed the Shockley–Queisser limit. Triplet excited states are key intermediates in singlet fission and molecular or nanocrystal-based photon upconversion, multi-excitonic processes that can optimize the use of sunlight, in particular the energy contained in the green and NIR wavelengths, respectively. As described in the first section, the parameters affecting TET closely mirror those affecting charge transport in organic semiconductors, especially if CT intermediates are involved. Over the past 30 years, much progress has been made to understand the factors affecting the charge mobility in optoelectronic devices based on these solution processable materials, including semiconductor nanocrystals, which, like organic materials, also have tightly bound Frenkel excitons. Therefore, it would be prudent to selectively apply the lessons learnt in optimizing the mobility in organic thin film transistors and the power conversion efficiency in organic photovoltaics to engineering thin films with long triplet diffusion lengths. In particular, the synthetic ease in tuning the molecular or nanocrystal structure should in principle enhance the wavefunction or the orbital overlap between donors and acceptors, while maintaining control of the appropriate energy offsets, depending on whether exciton or charge transport is desired.

In terms of material design and synthesis, the challenge is to maximize the electronic coupling in the thin film over distances exceeding infinity in terms of molecular dimensions. This can be achieved by eliminating defects, whether at the grain boundaries in organic semiconductors, the mid-gap states in semiconductor nanocrystals, or dislocations in MOFs or COFs and other unintentional impurities in the thin film. While oxygen must be eliminated to prevent quenching of triplet excitons, it may be possible to use oxygen barriers that are already commercially available, *e.g.* polyisobutylene,[134,135] or the barrier layers used in the commercial production of OPV cells.

Solutions to the challenges in transporting triplet excitons in the thin film must bridge traditional disciplines. In terms of theory, Skourtis and Beratan have recently proposed an alternative mechanism to TET involving the simultaneous transfer of both the hole and the electron comprising the triplet exciton, eschewing ionic intermediates.[51] Their calculations suggest that this alternative mechanism may be favored for long bridges energetically resonant between donors and acceptors. Clearly, it will be up to spectroscopists and synthetic chemists to build and characterize systems that support this theoretical prediction. The development of new spectroscopic tools to visualize and quantify the contributions of singlet and triplet excitons to the transport in thin films is invaluable. Current investigations into the intermediates in singlet fission, *e.g.* bound triplet pair excimers[99] or strongly interacting triplet pairs,[136] *etc.*, enabled by various monomer or dimer configurations[97,137–142] will shed light on the dielectric environment needed to stabilize triplet excitons. Such interdisciplinary approaches will reveal the fundamental structure–property relationships affecting triplet diffusion in thin films, and ultimately enable the engineering of optoelectronic devices making use of multi-excitonic processes.

Acknowledgements

MLT acknowledges support from the Alfred P. Sloan Foundation and federal agencies like the Department of Defence and the National Science Foundation (ARO W911NF-14-1-0260 and NSF CHE-1351663).

References

1 P. Horton and A. Ruban, *J. Exp. Bot.*, 2005, **56**, 365–373.
2 H. Uoyama, K. Goushi, K. Shizu, H. Nomura and C. Adachi, *Nature*, 2012, **492**, 234–238.
3 H. Tanaka, K. Shizu, H. Miyazaki and C. Adachi, *Chem. Commun.*, 2012, **48**, 11392–11394.
4 A. Endo, M. Ogasawara, A. Takahashi, D. Yokoyama, Y. Kato and C. Adachi, *Adv. Mater.*, 2009, **21**, 4802–4806.
5 T. Nakagawa, S.-Y. Ku, K.-T. Wong and C. Adachi, *Chem. Commun.*, 2012, **48**, 9580–9582.
6 C. Adachi, M. A. Baldo, S. R. Forrest, S. Lamansky, M. E. Thompson and R. C. Kwong, *Appl. Phys. Lett.*, 2001, **78**, 1622–1624.
7 C. Adachi, M. A. Baldo, S. R. Forrest and M. E. Thompson, *Appl. Phys. Lett.*, 2000, **77**, 904–906.
8 C. Adachi, M. A. Baldo, M. E. Thompson and S. R. Forrest, *J. Appl. Phys.*, 2001, **90**, 5048–5051.
9 S. Lamansky, P. Djurovich, D. Murphy, F. Abdel-Razzaq, H.-E. Lee, C. Adachi, P. E. Burrows, S. R. Forrest and M. E. Thompson, *J. Am. Chem. Soc.*, 2001, **123**, 4304–4312.
10 M. B. Smith and J. Michl, *Annu. Rev. Phys. Chem.*, 2013, **64**, 361–386.
11 M. W. Wilson, A. Rao, B. Ehrler and R. H. Friend, *Acc. Chem. Res.*, 2013, **46**, 1330–1338.
12 D. N. Congreve, J. Lee, N. J. Thompson, E. Hontz, S. R. Yost, P. D. Reusswig, M. E. Bahlke, S. Reineke, T. Van Voorhis and M. A. Baldo, *Science*, 2013, **340**, 334–337.
13 B. Ehrler, M. W. Wilson, A. Rao, R. H. Friend and N. C. Greenham, *Nano Lett.*, 2012, **12**, 1053–1057.
14 A. Monguzzi, S. M. Borisov, J. Pedrini, I. Klimant, M. Salvalaggio, P. Biagini, F. Melchiorre, C. Lelii and F. Meinardi, *Adv. Funct. Mater.*, 2015, **25**, 5617–5624.
15 M. Mahboub, Z. Huang and M. L. Tang, *Nano Lett.*, 2016, **16**, 7169–7175.
16 M. Wu, D. N. Congreve, M. W. Wilson, J. Jean, N. Geva, M. Welborn, T. Van Voorhis, V. Bulović, M. G. Bawendi and M. A. Baldo, *Nat. Photonics*, 2016, **10**, 31–34.

17 M. A. Green, *Solar cells: operating principles, technology, and system applications*, Prentice-Hall, Inc., Englewood Cliffs, NJ, 1982.
18 D. V. Talapin, J.-S. Lee, M. V. Kovalenko and E. V. Shevchenko, *Chem. Rev.*, 2009, **110**, 389–458.
19 X. Li, V. M. Nichols, D. Zhou, C. Lim, G. S. H. Pau, C. J. Bardeen and M. L. Tang, *Nano Lett.*, 2014, **14**, 3382–3387.
20 M. Nirmal, D. J. Norris, M. Kuno, M. G. Bawendi, A. L. Efros and M. Rosen, *Phys. Rev. Lett.*, 1995, **75**, 3728.
21 N. J. Thompson, M. W. Wilson, D. N. Congreve, P. R. Brown, J. M. Scherer, T. S. Bischof, M. Wu, N. Geva, M. Welborn and T. Van Voorhis, *Nat. Mater.*, 2014, **13**, 1039–1043.
22 M. Tabachnyk, B. Ehrler, S. Gélinas, M. L. Böhm, B. J. Walker, K. P. Musselman, N. C. Greenham, R. H. Friend and A. Rao, *Nat. Mater.*, 2014, **13**, 1033–1038.
23 A. Rao, P. C. Chow, S. Gélinas, C. W. Schlenker, C.-Z. Li, H.-L. Yip, A. K.-Y. Jen, D. S. Ginger and R. H. Friend, *Nature*, 2013, **500**, 435–439.
24 P. C. Chow, S. Gélinas, A. Rao and R. H. Friend, *J. Am. Chem. Soc.*, 2014, **136**, 3424–3429.
25 S. Westenhoff, I. A. Howard, J. M. Hodgkiss, K. R. Kirov, H. A. Bronstein, C. K. Williams, N. C. Greenham and R. H. Friend, *J. Am. Chem. Soc.*, 2008, **130**, 13653–13658.
26 T. M. Clarke and J. R. Durrant, *Chem. Rev.*, 2010, **110**, 6736–6767.
27 C. W. Schlenker, K.-S. Chen, H.-L. Yip, C.-Z. Li, L. R. Bradshaw, S. T. Ochsenbein, F. Ding, X. S. Li, D. R. Gamelin and A. K.-Y. Jen, *J. Am. Chem. Soc.*, 2012, **134**, 19661–19668.
28 M. Liedtke, A. Sperlich, H. Kraus, A. Baumann, C. Deibel, M. J. Wirix, J. Loos, C. M. Cardona and V. Dyakonov, *J. Am. Chem. Soc.*, 2011, **133**, 9088–9094.
29 S. D. Dimitrov, S. Wheeler, D. Niedzialek, B. C. Schroeder, H. Utzat, J. M. Frost, J. Yao, A. Gillett, P. S. Tuladhar and I. McCulloch, *Nat. Commun*, 2015, **6**, 6501.
30 Z. Huang, X. Li, M. Mahboub, K. M. Hanson, V. M. Nichols, H. Le, M. L. Tang and C. J. Bardeen, *Nano Lett.*, 2015, **15**, 5552–5557.
31 Z. Huang, X. Li, B. D. Yip, J. M. Rubalcava, C. J. Bardeen and M. L. Tang, *Chem. Mater.*, 2015, **27**, 7503–7507.
32 Z. Huang, D. E. Simpson, M. Mahboub, X. Li and M. L. Tang, *Chem. Sci.*, 2016, **7**, 4101–4104.
33 X. Li, Z. Huang, R. Zavala and M. L. Tang, *J. Phys. Chem. Lett.*, 2016, **7**, 1955–1959.
34 C. Mongin, S. Garakyaraghi, N. Razgoniaeva, M. Zamkov and F. N. Castellano, *Science*, 2016, **351**, 369–372.
35 P. Xia, Z. Huang, X. Li, J. J. Romero, V. I. Vullev, G. S. H. Pau and M. L. Tang, *Chem. Commun.*, 2017, **53**, 1241–1244.
36 M. Mahboub, H. Maghsoudiganjeh, A. M. Pham, Z. Huang and M. L. Tang, *Adv. Funct. Mater.*, 2016, **26**, 6091–6097.
37 S. R. Yost, E. Hontz, S. Yeganeh and T. Van Voorhis, *J. Phys. Chem. C*, 2012, **116**, 17369–17377.
38 D. L. Dexter, *J. Chem. Phys.*, 1953, **21**, 836–850.
39 M. Pope and C. E. Swenberg, *Electronic processes in organic crystals and polymers*, Oxford University Press, 1999.
40 J. A. Freund and T. Poschel, *Stochastic Processes in Physics, Chemistry, Biology*, Springer, 2000.
41 R. A. Marcus, *J. Chem. Phys.*, 1956, **24**, 966–978.
42 R. A. Marcus, *Rev. Mod. Phys.*, 1993, **65**, 599.
43 R. A. Marcus and N. Sutin, *Biochim. Biophys. Acta, Rev. Bioenerg.*, 1985, **811**, 265–322.
44 A. Köhler and H. Bässler, *J. Mater. Chem.*, 2011, **21**, 4003–4011.
45 R. D. Harcourt, G. D. Scholes and K. P. Ghiggino, *J. Chem. Phys.*, 1994, **101**, 10521–10525.
46 G. L. Closs, M. D. Johnson, J. R. Miller and P. Piotrowiak, *J. Am. Chem. Soc.*, 1989, **111**, 3751–3753.
47 G. L. Closs, P. Piotrowiak, J. M. MacInnis and G. R. Fleming, *J. Am. Chem. Soc.*, 1988, **110**, 2652–2653.
48 B. P. Krueger, G. D. Scholes and G. R. Fleming, *J. Phys. Chem. B*, 1998, **102**, 5378–5386.
49 G. D. Scholes and K. P. Ghiggino, *J. Phys. Chem.*, 1994, **98**, 4580–4590.
50 G. D. Scholes, *J. Phys. Chem.*, 1996, **100**, 18731–18739.
51 S. S. Skourtis, C. Liu, P. Antoniou, A. M. Virshup and D. N. Beratan, *Proc. Natl. Acad. Sci. U. S. A.*, 2016, **113**, 8115–8120.
52 R. R. Lunt, N. C. Giebink, A. A. Belak, J. B. Benziger and S. R. Forrest, *J. Appl. Phys.*, 2009, **105**, 053711.
53 W. Zhang, J. Yu, W. Wen and Y. Jiang, *J. Lumin.*, 2011, **131**, 1260–1263.
54 J. Wünsche, S. Reineke, B. Lüssem and K. Leo, *Phys. Rev. B: Condens. Matter Mater. Phys.*, 2010, **81**, 245201.
55 H. Najafov, B. Lee, Q. Zhou, L. Feldman and V. Podzorov, *Nat. Mater.*, 2010, **9**, 938–943.
56 P. Irkhin and I. Biaggio, *Phys. Rev. Lett.*, 2011, **107**, 017402.
57 J. Lee, P. Jadhav, P. D. Reusswig, S. R. Yost, N. J. Thompson, D. N. Congreve, E. Hontz, T. Van Voorhis and M. A. Baldo, *Acc. Chem. Res.*, 2013, **46**, 1300–1311.
58 J. J. Burdett and C. J. Bardeen, *Acc. Chem. Res.*, 2013, **46**, 1312–1320.
59 J. R. Ochsmann, D. Chandran, D. W. Gehrig, H. Anwar, P. K. Madathil, K. S. Lee and F. Laquai, *Macromol. Rapid Commun.*, 2015, **36**, 1122–1128.
60 R. J. Dillon, G. B. Piland and C. J. Bardeen, *J. Am. Chem. Soc.*, 2013, **135**, 17278–17281.
61 J. J. Burdett, A. M. Müller, D. Gosztola and C. J. Bardeen, *J. Chem. Phys.*, 2010, **133**, 144506.
62 J. J. Burdett and C. J. Bardeen, *J. Am. Chem. Soc.*, 2012, **134**, 8597–8607.
63 N. Giebink, Y. Sun and S. Forrest, *Org. Electron.*, 2006, **7**, 375–386.
64 M. Lebental, H. Choukri, S. Chenais, S. Forget, A. Siove, B. Geffroy and E. Tutiš, *Phys. Rev. B: Condens. Matter Mater. Phys.*, 2009, **79**, 165318.
65 N. Matsusue, S. Ikame, Y. Suzuki and H. Naito, *J. Appl. Phys.*, 2005, **97**, 123512.
66 B. W. D'Andrade, R. J. Holmes and S. R. Forrest, *Adv. Mater.*, 2004, **16**, 624–628.
67 T. Fushimi, A. Oda, H. Ohkita and S. Ito, *J. Phys. Chem. B*, 2004, **108**, 18897–18902.
68 Y. Shao and Y. Yang, *Adv. Mater.*, 2005, **17**, 2841–2844.
69 V. Cleave, G. Yahioglu, P. L. Barny, R. H. Friend and N. Tessler, *Adv. Mater.*, 1999, **11**, 285–288.
70 M. Baldo, D. O'brien, M. Thompson and S. Forrest, *Phys. Rev. B: Condens. Matter Mater. Phys.*, 1999, **60**, 14422.
71 O. V. Mikhnenko, R. Ruiter, P. W. Blom and M. A. Loi, *Phys. Rev. Lett.*, 2012, **108**, 137401.
72 M. Tabachnyk, B. Ehrler, S. Bayliss, R. H. Friend and N. C. Greenham, *Appl. Phys. Lett.*, 2013, **103**, 190–191.
73 D. Qin, P. Gu, R. S. Dhar, S. G. Razavipour and D. Ban, *Phys. Status Solidi A*, 2011, **208**, 1967–1971.
74 W. A. Luhman and R. J. Holmes, *Appl. Phys. Lett.*, 2009, **94**, 110.
75 B. P. Rand, S. Schols, D. Cheyns, H. Gommans, C. Girotto, J. Genoe, P. Heremans and J. Poortmans, *Org. Electron.*, 2009, **10**, 1015–1019.
76 G. Vaubel and H. Kallmann, *Phys. Status Solidi B*, 1969, **35**, 789–792.
77 W. Hofberger and H. Bässler, *Phys. Status Solidi B*, 1975, **69**, 725–730.
78 G. Schwartz, S. Reineke, T. C. Rosenow, K. Walzer and K. Leo, *Adv. Funct. Mater.*, 2009, **19**, 1319–1333.
79 S. C. Meskers, J. Hübner, M. Oestreich and H. Bässler, *J. Phys. Chem. B*, 2001, **105**, 9139–9149.
80 G. M. Akselrod, P. B. Deotare, N. J. Thompson, J. Lee, W. A. Tisdale, M. A. Baldo, V. M. Menon and V. Bulović, *Nat. Commun.*, 2014, **5**, 1–8.
81 Y. Wan, Z. Guo, T. Zhu, S. Yan, J. Johnson and L. Huang, *Nat. Chem.*, 2015, **7**, 785–792.
82 T. Zhu, Y. Wan, Z. Guo, J. Johnson and L. Huang, *Adv. Mater.*, 2016, **28**, 7539–7547.
83 S. J. Yoon, Z. Guo, P. C. dos Santos Claro, E. V. Shevchenko and L. Huang, *ACS Nano*, 2016, **10**, 7208–7215.
84 W. Zhang, J. Smith, S. E. Watkins, R. Gysel, M. McGehee, A. Salleo, J. Kirkpatrick, S. Ashraf, T. Anthopoulos and M. Heeney, *J. Am. Chem. Soc.*, 2010, **132**, 11437–11439.
85 H. Sirringhaus, P. Brown, R. Friend, M. M. Nielsen, K. Bechgaard, B. Langeveld-Voss, A. Spiering, R. A. Janssen, E. Meijer and P. Herwig, *Nature*, 1999, **401**, 685–688.
86 D. P. McMahon, D. L. Cheung, L. Goris, J. Dacuña, A. Salleo and A. Troisi, *J. Phys. Chem. C*, 2011, **115**, 19386–19393.
87 J. Rivnay, M. F. Toney, Y. Zheng, I. V. Kauvar, Z. Chen, V. Wagner, A. Facchetti and A. Salleo, *Adv. Mater.*, 2010, **22**, 4359–4363.
88 A. Facchetti, *Chem. Mater.*, 2010, **23**, 733–758.
89 H. Yan, Z. Chen, Y. Zheng, C. Newman, J. R. Quinn, F. Dötz, M. Kastler and A. Facchetti, *Nature*, 2009, **457**, 679–686.
90 R. Noriega, J. Rivnay, K. Vandewal, F. P. Koch, N. Stingelin, P. Smith, M. F. Toney and A. Salleo, *Nat. Mater.*, 2013, **12**, 1038–1044.
91 W. Ma, C. Yang, X. Gong, K. Lee and A. J. Heeger, *Adv. Funct. Mater.*, 2005, **15**, 1617–1622.
92 B. M. Savoie, A. Rao, A. A. Bakulin, S. Gelinas, B. Movaghar, R. H. Friend, T. J. Marks and M. A. Ratner, *J. Am. Chem. Soc.*, 2014, **136**, 2876–2884.

93 L. Leibler, *Macromolecules*, 1980, **13**, 1602–1617.
94 E. W. Cochran, C. J. Garcia-Cervera and G. H. Fredrickson, *Macromolecules*, 2006, **39**, 2449–2451.
95 F. S. Bates and G. H. Fredrickson, *Phys. Today*, 1999, **52**, 32–38.
96 F. S. Bates and G. H. Fredrickson, *Annu. Rev. Phys. Chem.*, 1990, **41**, 525–557.
97 S. N. Sanders, E. Kumarasamy, A. B. Pun, M. L. Steigerwald, M. Y. Sfeir and L. M. Campos, *Angew. Chem.*, 2016, **128**, 3434–3438.
98 S. N. Sanders, E. Kumarasamy, A. B. Pun, M. T. Trinh, B. Choi, J. L. Xia, E. J. Taffet, J. Z. Low, J. R. Miller, X. Roy, X. Y. Zhu, M. L. Steigerwald, M. Y. Sfeir and L. M. Campos, *J. Am. Chem. Soc.*, 2015, **137**, 8965–8972.
99 H. L. Stern, A. J. Musser, S. Gelinas, P. Parkinson, L. M. Herz, M. J. Bruzek, J. Anthony, R. H. Friend and B. J. Walker, *Proc. Natl. Acad. Sci. U. S. A.*, 2015, **112**, 7656–7661.
100 C. Guo, Y.-H. Lin, M. D. Witman, K. A. Smith, C. Wang, A. Hexemer, J. Strzalka, E. D. Gomez and R. Verduzco, *Nano Lett.*, 2013, **13**, 2957–2963.
101 Y. Lee and E. D. Gomez, *Macromolecules*, 2015, **48**, 7385–7395.
102 A. Monguzzi, M. Mauri, M. Frigoli, J. Pedrini, R. Simonutti, C. Larpent, G. Vaccaro, M. Sassi and F. Meinardi, *J. Phys. Chem. Lett.*, 2016, **7**, 2779–2785.
103 A. Monguzzi, J. Mezyk, F. Scotognella, R. Tubino and F. Meinardi, *Phys. Rev. B: Condens. Matter Mater. Phys.*, 2008, **78**, 195112.
104 P. Duan, N. Yanai and N. Kimizuka, *J. Am. Chem. Soc.*, 2013, **135**, 19056–19059.
105 S. Hisamitsu, N. Yanai and N. Kimizuka, *Angew. Chem., Int. Ed.*, 2015, **54**, 11550–11554.
106 T. Ogawa, N. Yanai, A. Monguzzi and N. Kimizuka, *Sci. Rep.*, 2015, **5**, 10882.
107 J. R. Lakowicz, *Principles of fluorescence spectroscopy*, Springer, 3rd edn, 2006.
108 F. Marsico, A. Turshatov, R. Peköz, Y. Avlasevich, M. Wagner, K. Weber, D. Donadio, K. Landfester, S. Baluschev and F. R. Wurm, *J. Am. Chem. Soc.*, 2014, **136**, 11057–11064.
109 S. Baluschev, K. Katta, Y. Avlasevich and K. Landfester, *Mater. Horiz.*, 2016, **3**, 478–486.
110 H. Kouno, T. Ogawa, S. Amemori, P. Mahato, N. Yanai and N. Kimizuka, *Chem. Sci.*, 2016, **7**, 5224–5229.
111 C. A. Kent, B. P. Mehl, L. Ma, J. M. Papanikolas, T. J. Meyer and W. Lin, *J. Am. Chem. Soc.*, 2010, **132**, 12767–12769.
112 C. A. Kent, D. Liu, L. Ma, J. M. Papanikolas, T. J. Meyer and W. Lin, *J. Am. Chem. Soc.*, 2011, **133**, 12940–12943.
113 C. A. Kent, D. Liu, T. J. Meyer and W. Lin, *J. Am. Chem. Soc.*, 2012, **134**, 3991–3994.
114 J. Lin, X. Hu, P. Zhang, A. Van Rynbach, D. N. Beratan, C. A. Kent, B. P. Mehl, J. M. Papanikolas, T. J. Meyer and W. Lin, *J. Phys. Chem. C*, 2013, **117**, 22250–22259.
115 Q. Zhang, C. Zhang, L. Cao, Z. Wang, B. An, Z. Lin, R. Huang, Z. Zhang, C. Wang and W. Lin, *J. Am. Chem. Soc.*, 2016, **138**, 5308–5315.
116 W. A. Maza, R. Padilla and A. J. Morris, *J. Am. Chem. Soc.*, 2015, **137**, 8161–8168.
117 M. Oldenburg, A. Turshatov, D. Busko, S. Wollgarten, M. Adams, N. Baroni, A. Welle, E. Redel, C. Wöll and B. S. Richards, *Adv. Mater.*, 2016, **28**, 8477–8482.
118 P. Mahato, N. Yanai, M. Sindoro, S. Granick and N. Kimizuka, *J. Am. Chem. Soc.*, 2016, **138**, 6541–6549.
119 X. Feng, X. Ding, L. Chen, Y. Wu, L. Liu, M. Addicoat, S. Irle, Y. Dong and D. Jiang, *Sci. Rep.*, 2016, **6**, 32944.
120 L. Chen, K. Furukawa, J. Gao, A. Nagai, T. Nakamura, Y. Dong and D. Jiang, *J. Am. Chem. Soc.*, 2014, **136**, 9806–9809.
121 S. Jin, M. Supur, M. Addicoat, K. Furukawa, L. Chen, T. Nakamura, S. Fukuzumi, S. Irle and D. Jiang, *J. Am. Chem. Soc.*, 2015, **137**, 7817–7827.
122 S. Jin, K. Furukawa, M. Addicoat, L. Chen, S. Takahashi, S. Irle, T. Nakamura and D. Jiang, *Chem. Sci.*, 2013, **4**, 4505–4511.
123 X. Ding, L. Chen, Y. Honsho, X. Feng, O. Saengsawang, J. Guo, A. Saeki, S. Seki, S. Irle and S. Nagase, *J. Am. Chem. Soc.*, 2011, **133**, 14510–14513.
124 D. D. Medina, V. Werner, F. Auras, R. Tautz, M. Dogru, J. r. Schuster, S. Linke, M. Döblinger, J. Feldmann and P. Knochel, *ACS Nano*, 2014, **8**, 4042–4052.
125 M. Dogru, M. Handloser, F. Auras, T. Kunz, D. Medina, A. Hartschuh, P. Knochel and T. Bein, *Angew. Chem., Int. Ed.*, 2013, **52**, 2920–2924.
126 J. Guo, Y. Xu, S. Jin, L. Chen, T. Kaji, Y. Honsho, M. A. Addicoat, J. Kim, A. Saeki and H. Ihee, *Nat. Commun.*, 2013, **4**, 2736.
127 N. Geacintov, M. Pope and F. Vogel, *Phys. Rev. Lett.*, 1969, **22**, 593.
128 R. Groff, A. Suna, P. Avakian and R. Merrifield, *Phys. Rev. B: Solid State*, 1974, **9**, 2655.
129 B. Ehrler, B. J. Walker, M. L. Boehm, M. W. B. Wilson, Y. Vaynzof, R. H. Friend and N. C. Greenham, *Nat. Commun.*, 2012, **3**, 1019.
130 B. Ehrler, M. W. B. Wilson, A. Rao, R. H. Friend and N. C. Greenham, *Nano Lett.*, 2012, **12**, 1053–1057.
131 L. Yang, M. Tabachnyk, S. L. Bayliss, M. L. Boehm, K. Broch, N. C. Greenham, R. H. Friend and B. Ehrler, *Nano Lett.*, 2015, **15**, 354–358.
132 W.-L. Chan, M. Ligges, A. Jailaubekov, L. Kaake, L. Miaja-Avila and X. Y. Zhu, *Science*, 2011, **334**, 1541–1545.
133 A. Rao, P. C. Y. Chow, S. Gelinas, C. W. Schlenker, C.-Z. Li, H.-L. Yip, A. K. Y. Jen, D. S. Ginger and R. H. Friend, *Nature*, 2013, **500**, 435–439.
134 K. Kunal, M. Paluch, C. Roland, J. Puskas, Y. Chen and A. Sokolov, *J. Polym. Sci., Part B: Polym. Phys.*, 2008, **46**, 1390–1399.
135 A. Vohra, R. S. Carmichael and T. B. Carmichael, *Langmuir*, 2016, **32**, 10206–10212.
136 R. D. Pensack, E. E. Ostroumov, A. J. Tilley, S. Mazza, C. Grieco, K. J. Thorley, J. B. Asbury, D. S. Seferos, J. E. Anthony and G. D. Scholes, *J. Phys. Chem. Lett.*, 2016, **7**, 2370–2375.
137 S. N. Sanders, E. Kumarasamy, A. B. Pun, M. T. Trinh, B. Choi, J. Xia, E. J. Taffet, J. Z. Low, J. R. Miller and X. Roy, *J. Am. Chem. Soc.*, 2015, **137**, 8965–8972.
138 N. V. Korovina, S. Das, Z. Nett, X. Feng, J. Joy, R. Haiges, A. I. Krylov, S. E. Bradforth and M. E. Thompson, *J. Am. Chem. Soc.*, 2016, **138**, 617–627.
139 J. Zirzlmeier, D. Lehnherr, P. B. Coto, E. T. Chernick, R. Casillas, B. S. Basel, M. Thoss, R. R. Tykwinski and D. M. Guldi, *Proc. Natl. Acad. Sci. U. S. A.*, 2015, **112**, 5325–5330.
140 S. Lukman, A. J. Musser, K. Chen, S. Athanasopoulos, C. K. Yong, Z. Zeng, Q. Ye, C. Chi, J. M. Hodgkiss and J. Wu, *Adv. Funct. Mater.*, 2015, **25**, 5452–5461.
141 B. Ehrler, B. J. Walker, M. L. Böhm, M. W. Wilson, Y. Vaynzof, R. H. Friend and N. C. Greenham, *Nat. Commun.*, 2012, **3**, 1019.
142 Y.-D. Zhang, Y. Wu, Y. Xu, Q. Wang, K. Liu, J.-W. Chen, J.-J. Cao, C. Zhang, H. Fu and H.-L. Zhang, *J. Am. Chem. Soc.*, 2016, **138**, 6739–6745.

